© 2018. Published by The Company of Biologists Ltd | Development (2018) 145, dev169326. doi:10.1242/dev.169326

RESEARCH REPORT

Centriole planar polarity assessment in *Drosophila* wings

Sergio Garrido-Jimenez[1,*], Angel-Carlos Roman[2,*], Alberto Alvarez-Barrientos[3] and Jose Maria Carvajal-Gonzalez[1,‡]

ABSTRACT

In vertebrates, planar polarization of ciliary basal bodies has been associated with actin polymerization that occurs downstream of the Frizzled-planar cell polarity (Fz-PCP) pathway. In *Drosophila* wing epithelial cells, which do not have cilia, centrioles also polarize in a Fz-PCP-dependent manner, although the relationship with actin polymerization remains unknown. By combining existing and new quantitative methods, we unexpectedly found that known PCP effectors linked to actin polymerization phenotypes affect neither final centriole polarization nor apical centriole distribution. But actin polymerization is required upstream of Fz-PCP to maintain the centrioles in restricted areas in the apical-most planes of those epithelial cells before and after the actin-based hair is formed. Furthermore, in the absence of proper core Fz-PCP signalling, actin polymerization is insufficient to drive this off-centred centriole migration. Altogether, the results reveal that there are at least two pathways controlling centriole positioning in *Drosophila* pupal wings – an upstream actin-dependent mechanism involved in centriole distribution that is PCP independent, and an unknown mechanism that links core Fz-PCP and centriole polarization.

KEY WORDS: Centrioles, Planar cell polarity, Frizzled, Actin polymerization, Planar cell polarity effectors

INTRODUCTION

In some specialized epithelial cells, polarized settling of a centriole at the core of the ciliary basal body is essential for coordinated cilia beating (Brooks and Wallingford, 2014; Ohata and Alvarez-Buylla, 2016; Spassky and Meunier, 2017). Excellent examples are multiciliated cells lining the oviduct, brain ventricles, and the airway tract, in which coordinated arrangement between neighbouring basal bodies within the same cell is key to creating directional movement of ovules, cerebrospinal fluid flow and mucus, respectively (Brooks and Wallingford, 2014; Spassky and Meunier, 2017). Thus, deeper insights into the molecular mechanisms that control centriole positioning at the core of the ciliary basal body would have important implications for understanding the physiology and aetiology of pathological states coming from centriole mis-positioning (Bettencourt-Dias et al., 2011; Reiter and Leroux, 2017; Spassky and Meunier, 2017).

[1]Departamento de Bioquímica, Biología Molecular y Genética, Facultad de Ciencias, Universidad de Extremadura, 06071 Badajoz, Spain. [2]Champalimaud Neuroscience Programme, Avenida de Brasilia, Lisbon 1400-038, Portugal. [3]Servicio de Técnicas Aplicadas a las Biociencias (STAB), Universidad de Extremadura, 06071 Badajoz, Spain.
*These authors contributed equally to this work

‡Author for correspondence (jmcarvaj@unex.es)

J.M., 0000-0001-6576-830X

Received 25 June 2018; Accepted 26 October 2018

The Frizzled (Fz) planar cell polarity pathway (PCP) is a conserved pathway governed by two protein complexes – the Frizzled/Dishevelled/Flamingo/Diego (Fz/Dsh/Fmi/Dgo) complex and the Vang/Prickle/Flamingo (Vang/Pk/Fmi) complex (Adler, 2012; Carvajal-Gonzalez and Mlodzik, 2014; Devenport, 2014; Goodrich and Strutt, 2011; Peng and Axelrod, 2012; Singh and Mlodzik, 2012). The main role of the Fz-PCP pathway during development is to coordinate cells within a tissue in different cellular processes. Recently, this pathway has been shown to be essential for proper translational polarity, which refers to the off-centre movement of centrioles, and/or rotational polarity, which refers to the position of a basal body relative to neighbouring basal bodies. Examples in multiciliated cells occur in the larval skin of *Xenopus*, mouse ependymal cells and mouse oviduct epithelial cells (Mitchell et al., 2009; Park et al., 2006, 2008; Guirao et al., 2010; Shi et al., 2014, 2016). Similarly, the positioning of cilia and their basal bodies is also regulated by the Fz-PCP pathway in the outer hair cells in the mouse cochlea (Ezan and Montcouquiol, 2013; Jones and Chen, 2008), the mouse node (Song et al., 2010) and the floor plate of zebrafish (Borovina et al., 2010). We have found previously that this centriole polarization function of the Fz-PCP pathway was evolutionarily conserved by showing that centriole polarity was also controlled by this pathway in *Drosophila* wings (Carvajal-Gonzalez et al., 2016a,b).

In vertebrates, the Fz-PCP pathway and basal body polarization link is mediated, at least in part, by the downstream CPLANE (ciliogenesis and planar polarity effector) complex, formed in part by Inturned (Intu), Fuzzy (Fuz) and WD repeat containing planar cell polarity effector (Wdpcp) (Adler and Wallingford, 2017; Park et al., 2006). This CPLANE complex was first discovered in *Drosophila*, with its components being termed PCP effectors (PPEs), including In (Inturned) (Park et al., 1996), Fy (Fuzzy) (Collier and Gubb, 1997) and Frtz (Fritz, Wdpcp in vertebrates) (Collier et al., 2005), *inter alia*. The CPLANE complex, together with Dvl (Dishevelled; Dsh in *Drosophila*) and RhoA (Rho1 in *Drosophila*), is involved in early stages of centriole positioning during ciliogenesis, strikingly affecting protein vesicular transport and the docking of centrioles to the apical membrane in vertebrates, which is related to actin polymerization defects (Gray et al., 2009; Mitchell et al., 2009; Park et al., 2006, 2008). Although PPEs deeply affect actin polymerization, their role in centriole polarization remains largely unexplored in *Drosophila*. In fact, the role of actin in centriole polarization downstream of the Fz-PCP pathway is unknown. In this sense, we have discovered previously that centriole planar polarization was very mildly affected in a *multiple wing hairs* mutant, the most downstream target of the PPE complex (Carvajal-Gonzalez et al., 2016b). Based on this initial result, we decided to study in more depth the connection between actin, known PPEs, and centriole polarization in *Drosophila* wings.

Development (2018) 145, dev169326. doi:10.1242/dev.169326

RESULTS AND DISCUSSION

Multiple hair cell phenotypes induced by PPE loss-of-function conditions do not affect centriole polarity

In adult and pupal *Drosophila* wings, such PCP phenotypes as hair number defects [multiple hair cell (mhc) phenotypes] or hair misorientation defects are linked to actin polymerization dysfunction that can present at the apical membrane of each epithelial cell (Carvajal-Gonzalez and Mlodzik, 2014; Wong and Adler, 1993). The mhc phenotypes are related to PPEs, including actin polymerization regulators downstream of the core Fz-PCP pathway (Fig. 1A), whereas hair misorientation is controlled by the core members of the Fz-PCP or Fat-PCP pathways (Carvajal-Gonzalez and Mlodzik, 2014; Wong and Adler, 1993). To study the involvement of PPE in centriole polarization, we first tested available RNA interference (RNAi) lines for each of the commonly known PPEs and detected those that generated robust mhc phenotypes in adult wings (Fig. 1B-E; Fig. S1). In our experimental conditions with Sas4-GFP combined with *dpp>Gal4*, RNAi lines for *mwh*, *frtz* and *Drok* (*Rok* – FlyBase) produced robust mhc phenotypes in adult and pupal wings (Fig. 1F-H″; Figs S1-S3). Once PCP phenotypes had been confirmed, we calculated centriole polarity by using two existing methods – the average basal body position (ABP) and the quartile (Q) method – and compared centriole polarity in PPE loss-of-function (LOF) versus wild-type (WT) conditions (Fig. 1I,J). Briefly, the ABP method is based on the normalized position of a centriole along the proximal-distal (P-D) axis of the cell, and the Q method quantifies the number of centrioles located within four angular regions (Q1-Q4) of a population of cells, with Q1 being the quartile that represents polarized centrioles (for more details, see Materials and Methods). Unexpectedly, cells with at least two hairs showed a WT polarity of centrioles in *frtz*-RNAi, *Drok*-RNAi and *mwh*-RNAi conditions using the ABP method (Fig. 1I). By contrast, the Q method showed a mild, but statistically significant, reduction in Q1 centriole

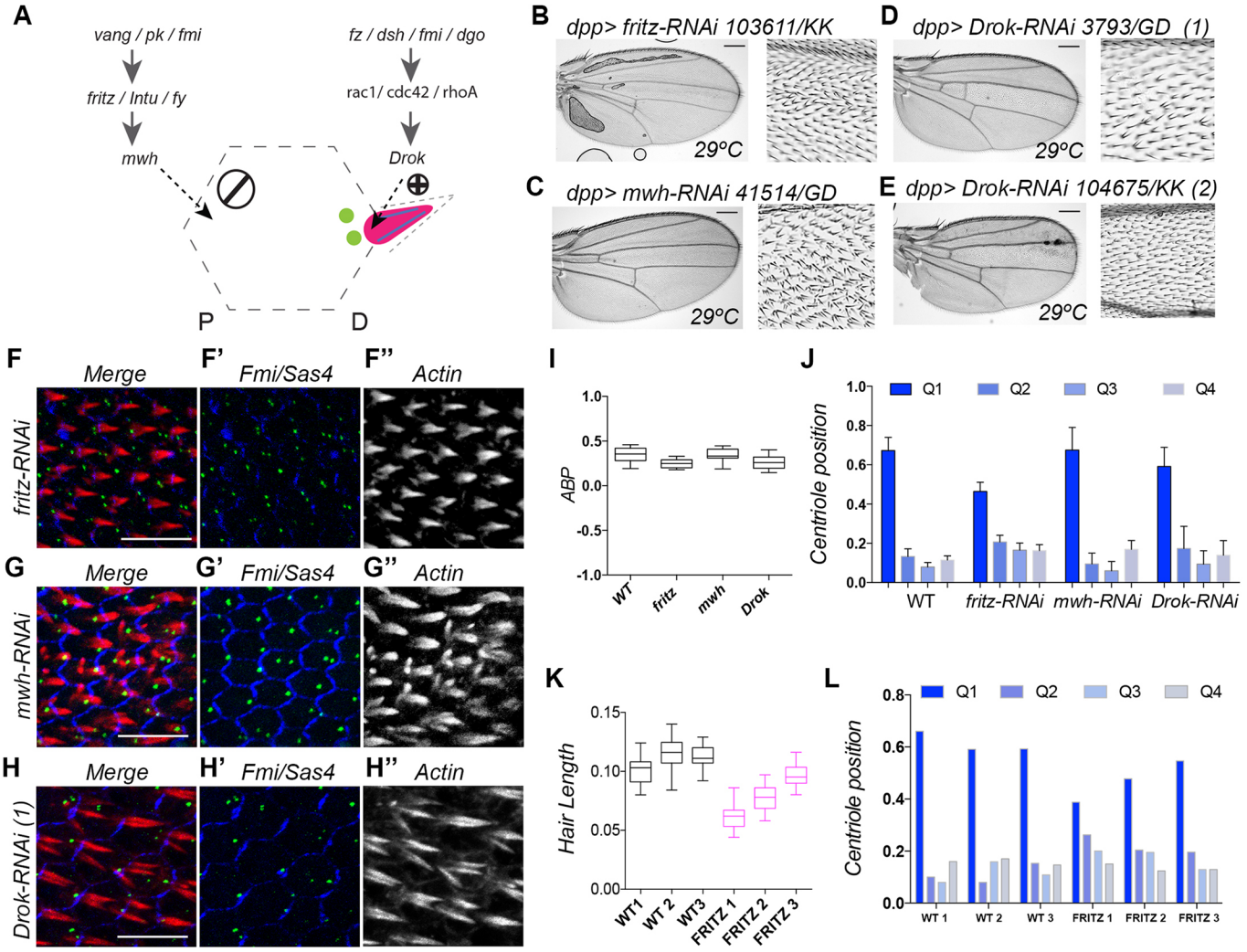

Fig. 1. Multiple hair cell phenotypes induced by PPE LOF conditions do not affect centriole polarity. (A) Schematic of core PCP and actin polymerization regulators. Green circles represent centrioles; blue lines are microtubules; the pink region is the actin based-hair. The PCP components related to inhibition or activation of actin polymerization are depicted in our model system. P, proximal side; D, distal side. (B-E) Multiple hair cell phenotypes confirmed in adult wings with RNAi against *frtz* (B), *mwh* (C) and *Drok* (D,E). (F-H″) Pupal wings with *frtz*-IR (F-F″), *mwh*-IR (G-G″) or *Drok*-IR (H-H″), showing Sas4-GFP (green), Fmi (blue) and actin (red/grey). (I,J) Centriole polarity calculated with ABP and Q methods in *frtz*-IR, *mwh*-IR and *Drok*-IR. The ABP method does not reveal differences between groups whereas the Q method shows a decrease in Q1 for *fritz*-IR. (K,L) Analyses of hair length and Q centriole positioning in paired WT-FRITZ conditions. 1, 2, 3 indicate different pupal wings. In I,K, box and whiskers represent median and 5-95 percentile. In J,L, error bars represent s.d. Number of cells>200 (at least four independent wings for each experimental condition). See Table S1 for statistical analysis. Scale bars: 250 µm in B-E; 10 µm in F-H.

Development (2018) 145, dev169326. doi:10.1242/dev.169326

positioning in *frtz*-RNAi conditions compared with WT, but no differences compared with WT in the *Drok*-RNAi and *mwh*-RNAi experiments (Fig. 1I,J; Table S1 for the statistical analyses). We also observed that *frtz*-RNAi produced a delay in hair formation with respect to the WT area of the same wing, which also correlates with a delay in centriole polarization (Fig. 1K,L; Fig. S2). This delay could also explain our former *mwh* mutant data (Carvajal-Gonzalez et al., 2016b), in which we found a mild effect on centriole polarity. Finally, we found that *Drok* knockdown also generated an increased cell size that did not affect centriole polarization (Fig. S3D).

Altogether, this data set indicates that the number of actin-rich hairs induced by PPE LOF might delay centriole polarity or cell size, but does not affect final centriole position. Our unexpected data on PPE seem to contradict the vertebrate data (Gray et al., 2009; Mitchell et al., 2009; Park et al., 2006, 2008). In vertebrates, the functional link between CPLANE proteins and Rho GTPases and ciliogenesis is very well-established and involves a decreased apical actin assembly, which is important for the orientation of basal bodies and cilia (Park et al., 2006, 2008). In flies, most of the PPE mutants (including *mwh*, *in*, *fy*, *frtz*, *Drok*, *Rac1*, *rho*) do not show any decreased or increased actin polymerization, and indeed it is believed that PPE mutants fail to restrict the actin polymerization site in the apical membrane. In any case, although this actin defect is present in PPE mutants, we found no effect on centriole polarity.

Actin polymerization is required to polarize centrioles

To determine whether or not actin polymerization is required for centriole polarization, we decided to block actin polymerization acutely by using drug treatment in *Drosophila* pupal wings *in vitro* (Fig. 2A). In our culturing conditions, 30-40% of pupal wings were able to fully develop up to the point of producing actin-rich hairs in each epithelial cell and distal wing fold (Fig. 2B-D). Again, using ABP and Q methods, pupal wings aged for 25 h at 29°C plus 10 h cultured *in vitro* showed partial centriole polarization compared with fully polarized centrioles [pupae aged up to 28.5 hours after puparium formation (APF)] or non-polarized centrioles (pupae aged up to 25 APF) (Fig. 2F,G). Under those *in vitro* culturing conditions causing a partial centriole polarization (25 APF plus 10 h culture *in vitro*), when actin polymerization was blocked by cytochalasin D treatment, we found that centriole polarization was completely inhibited (Fig. 2F,G; Table S2 for statistical analyses).

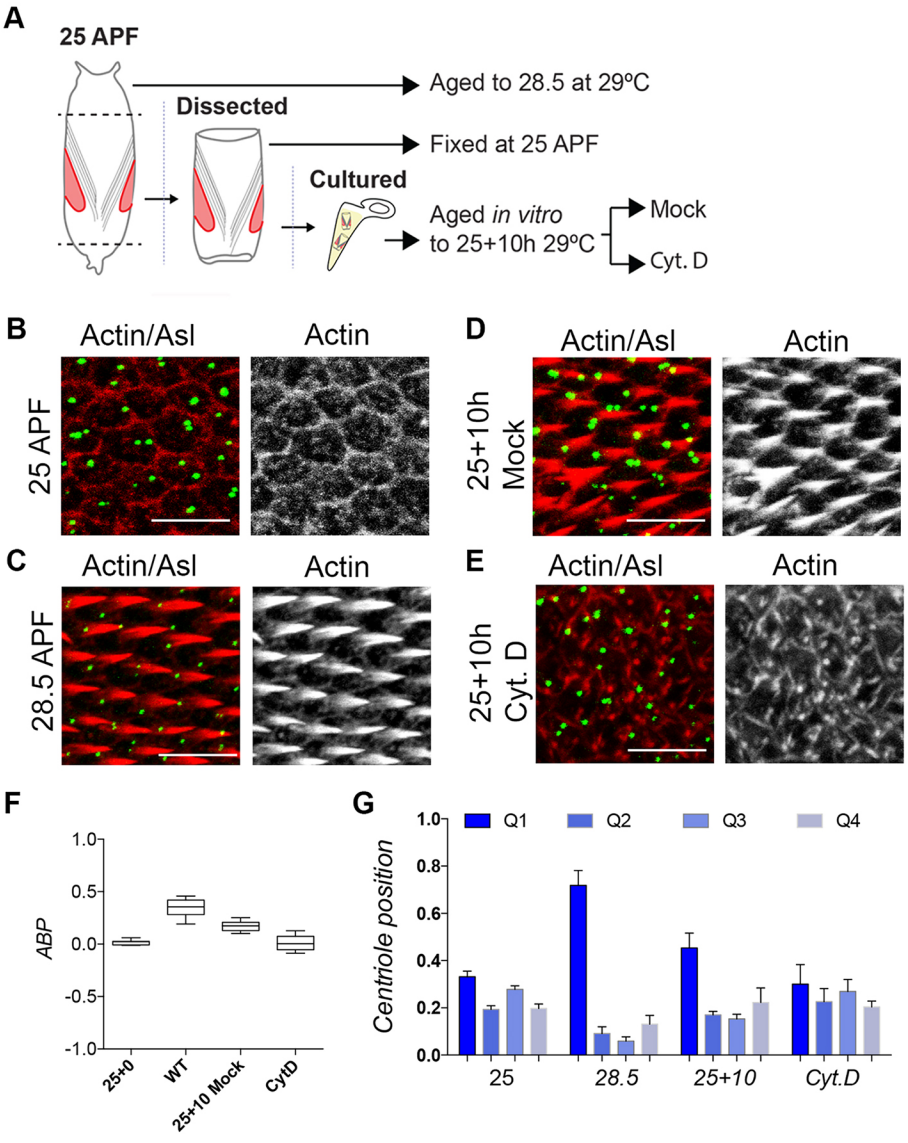

Fig. 2. Cytochalasin D affects centrioles polarization. (A) Schematic of the protocol followed to obtain pupal wings for *in vitro* experiments. (B-E) Confocal images for 25 APF (B), 28.5 APF (C), 25+10 h mock treatment (D) and 25+10 h cytochalasin D treatment (E) depicting centrioles in green (Asl-GFP) and actin in red/grey. (F,G) Centriole polarity analyses using ABP and Q methods in 25 APF, 28.5 APF, 25+10 h mock treatment and 25+10 h cytochalasin D treatment. In F, box and whiskers represent the median and 5-95 percentile. In G, error bars represent s.d. Number of cells>500 (at least 6 independent wings for each experimental condition). See Table S2 for statistical analysis. Cyt.D., cytochalasin D. Scale bars: 10 µm.

Development (2018) 145, dev169326. doi:10.1242/dev.169326

This result highlighted that actin polymerization is required for centriole polarization in *Drosophila* pupal wings, as has been reported for vertebrates previously.

Of the PPEs described, only Cdc42 LOF blocks actin-rich hair formation (Eaton et al., 1995, 1996), a phenotype that we were not able to obtain using available CDC42 stocks, but which is comparable to our cytochalasin D treatment. Furthermore, cytochalasin D interferes with basal body migration and ciliary development in epithelial cells by blocking actin filament formation (Boisvieux-Ulrich et al., 1990), and decreases centriole polarization in planarians (Almuedo-Castillo et al., 2011), and now we found that actin polymerization is required for centriole polarization. Therefore, although PPEs are not required for proper centriole polarization in *Drosophila*, actin polymerization is required, mimicking the actin and centriole linkage phenotype previously found in vertebrates.

Representative polarized centriole distribution as a method for comparing centriole polarity

Because we found that PPEs do not affect centriole polarity but actin polymerization is still required in this process, we next investigated whether or not centriole distribution was affected in the distal part of the cell under PPE mutant conditions. To this end, we first developed a better quantitative system with which to measure centriole distribution. In the past and in this study, we and others had measured centriole polarization by using either the distance and position relative to the centre of the cell or the angle of the vector connecting the centre of the cell and the centriole, as in the ABP and Q methods (Carvajal-Gonzalez et al., 2016b; Minegishi et al., 2017; Taniguchi et al., 2011). Although useful, these approaches do not take into consideration the fact that centriole polarization is at least two-dimensional, so there is extra information that could lead to the discovery of otherwise hidden differences. To respond to this question and improve our quantitative analysis, we developed a system to measure and compare the centriole population of a given experimental condition in two dimensions, which we termed the 'representative polarized centriole distribution' (RPCD) (Fig. S4).

The RPCD is based on the generation of a centriole positioning library in well-polarized epithelial cells (Fig. S4A-D). The accumulation of single centriole positions in a normalized epithelial cell model produces a density map representing the distribution and enrichment of centrioles (Fig. S4D). This density map can then be segmented using different isolines along which the probability of finding a centriole is the same (Fig. S4E,F). By using this approach, we obtained a model distribution for centrioles that can be used for comparisons between two populations of centrioles (Fig. S5; see Materials and Methods for more details). Briefly, for a given number of cells, we retrieved from our library a model distribution of well-polarized centrioles. This expected distribution was then confronted with the observed centriole coverage value in the experimental condition, and the ratio $R_{0.05}$ (observed/expected) will be greater than unity when centrioles are well polarized and less than unity when centrioles are not significantly polarized ($P<0.05$) (Fig. S5).

As a proof of principle for our RPCD method, we compared centrioles from WT wings before hair formation (25 APF), with pre-hairs or with well-formed hairs (28.5 APF). As shown in Fig. 3A, with the appearance of the actin-rich hairs in WT wings, centrioles polarized towards the distal part, going from non-planar polarized and centred in the apical membrane to planar polarized towards the distal part of the cell (Fig. 3A,B). Furthermore, when we evaluated centriole polarization using RPCD in Fz overexpression (Fz-OE) or *Vang* knockdown conditions, we confirmed that centriole polarization was disturbed with $R_{0.05}$ values being less than unity (Fig. 3C,D; Fig. S7A), obtaining results similar to those previously obtained with the ABP and the Q methods (Fig. S6; Table S3).

Using our RPCD method under PPE conditions, we found that the centriole distribution in the distal part of the cells is not different from that of WT cells with a $R_{0.05}$ greater than unity in *frtz*-RNAi, *Drok*-RNAi and *mwh*-RNAi conditions (Fig. 3E,F; Fig. S7). Taking our RPCD, ABP and Q methods data together, we conclude that neither centriole polarity nor centriole population distribution in the distal part of the cell are affected under PPE conditions.

Unexpectedly, when we applied the RPCD method to our *in vitro* experimental data in wings treated with cytochalasin D, we observed noticeable differences in the density map of centrioles in the cytochalasin D-treated wings compared with all the other conditions (Fig. 3G,H). We found that the distribution of centrioles in cytochalasin D-treated wings generates a density map that is more spread out and homogeneous in the apical planes of cells than the maps observed in Fz-OE, *vang*-RNAi or 'no-hair' conditions (Fig. 3; Fig. S7A-D). To confirm this new phenotype, we used another centriole distribution model for comparison, but in this case for a non-polarized centriole distribution using wings developed up to 25 APF, which we termed a representative non-polarized centriole distribution (RNCD) (Fig. S4H-J). We compared different non-polarized conditions (Fz-OE, *vang*-RNAi and cytochalasin D treatment) with the RNCD, and found that centriole distributions in wings treated with cytochalasin D were significantly different from the rest of the non-polarized conditions (Fig. 3I). Furthermore, quantification of the centriole distribution after short treatments with cytochalasin D before hairs are formed or after hair formation showed the same result: centrioles became dispersed at the apical planes of the cells (Fig. S7E,F). Altogether, our data indicate that actin is required to keep centrioles in a restricted area before and after centriole polarization takes place.

This new analysis using RNCD and RPCD methods highlighted that centriole distribution is affected by actin polymerization in a different manner than under Fz-OE or *vang*-RNAi experimental conditions. Under core PCP mutant conditions, centrioles do not polarize (compare core PCP results with RPCD) but remain restricted to the central area in the apical-most planes of the epithelial cell (compare core PCP with RNCP) (Fig. S4K). In contrast, in the cytochalasin D treatment, the centrioles did not polarize (compare the cytochalasin D results with RPCD) and became dispersed in the apical planes (compare the cytochalasin D results with RNCD) (Fig. S4K).

Centrioles and actin-rich hairs are disconnected under Fz GOF and Vang LOF conditions

Next, to analyse whether actin polymerization is sufficient to polarize centrioles, we went back to our hair misorientation phenotypes. Under Fz-PCP mutant conditions, actin polymerization still takes place in the apical membrane, but the actin-rich hair is generated at the wrong place within that membrane, which correlates with centriole distribution defects (Fig. S6). Under those circumstances, we wondered whether, under hair misorientation conditions, centrioles were still able to follow the actin-rich hair or were completely uncoupled (Fig. 4A,B). To answer this question, we measured the co-occurrence of the two structures, actin-rich hairs and centrioles, at the same angle (see Materials and Methods for details; Fig. 4C-G). We analysed the percentage of co-occurrence in cells with hair misorientation

Development (2018) 145, dev169326. doi:10.1242/dev.169326

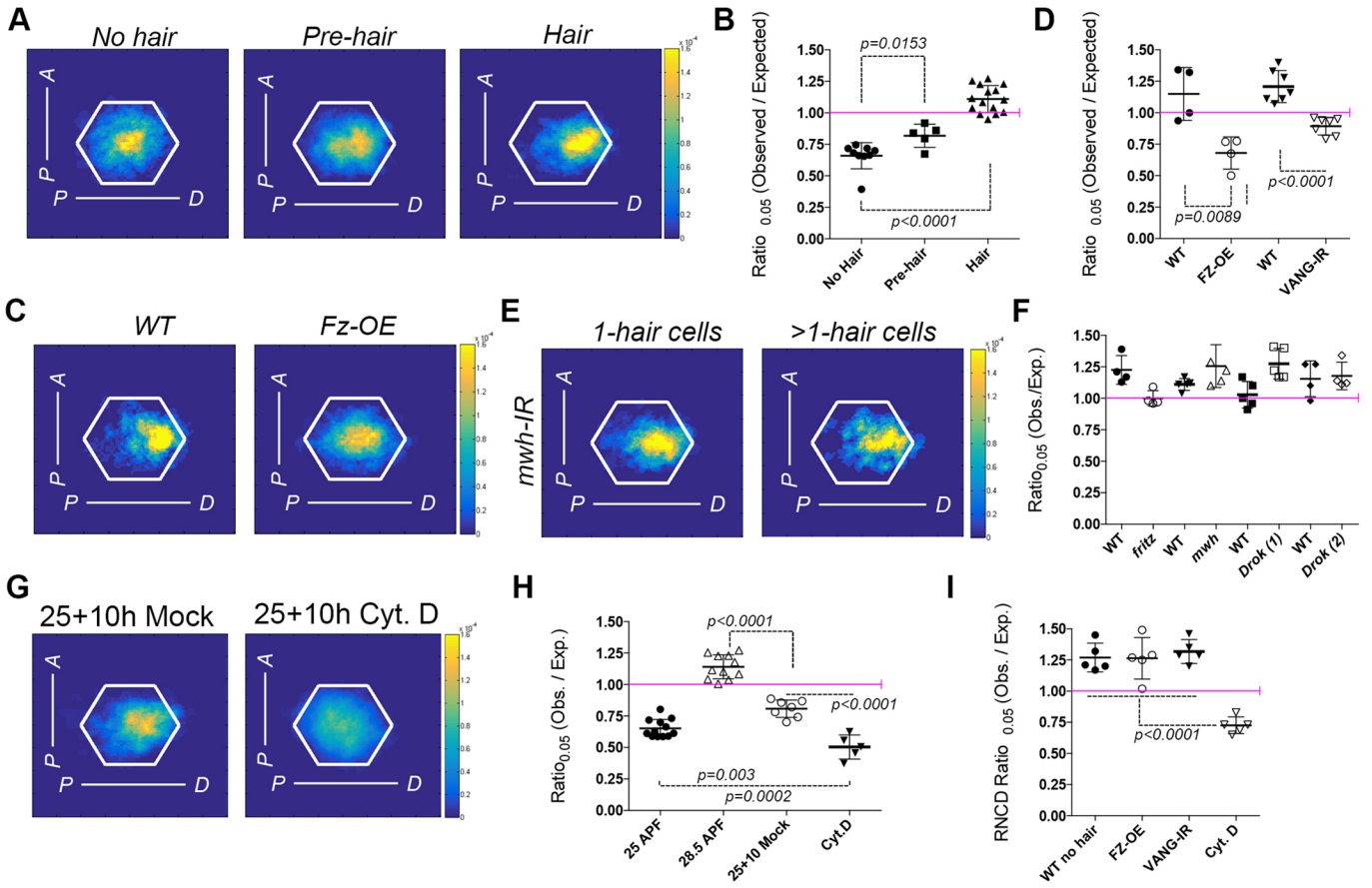

Fig. 3. Centriole polarity and distribution analyses measured and compared with the RPCD method. (A) Centriole density maps for no-hair, pre-hair and hair conditions in WT wings. P-A, posterior-anterior axis; P-D, proximal-distal axis. (B) Comparison of centriole polarity and distribution in no-hair, pre-hair and hair conditions in WT wings. (C) Centriole density maps for paired WT and Fz-OE conditions. (D) Comparison of centriole polarity and distribution using RPCD for Fz-OE and *vang*-RNAi conditions. (E) Centriole density maps for paired WT and *mwh*-IR cells. (F) Comparison of centriole polarity and distribution using RPCD for *frtz*-IR, *mwh*-IR and *Drok*-IR wings and paired WT cells. (G) Centriole density maps for paired *in vitro* wing cultures treated with cytochalasin D or mock treated. (H) Comparison of centriole polarity and distribution using RPCD for 25 APF, 28.5 APF, cytochalasin D and mock treatment conditions. (I) Comparison of centriole polarity and distribution using RNCD for WT no hairs, Fz-OE, *vang*-RNAi and cytochalasin D conditions. Error bars represent s.d. Number of cells>400 (at least five independent wings for each experimental condition). Cyt.D., cytochalasin D.

phenotypes using Fz-GOF (gain of function) and Vang-LOF conditions, but only in those cells in which centrioles were able to migrate towards the cell periphery. In all the conditions tested, cells with hair misorientation had a lower ability to locate centrioles at the base of the actin-rich hairs (Fig. 4H). These cells had 20% co-occurrence in Fz-GOF and 26% in Vang-LOF, both lower than the 46% estimated in WT cells (Fig. 4H). We concluded that, under PCP LOF and GOF conditions, the centriole loses its ability to follow the actin-rich hair positioning in the apical membrane of *Drosophila* wing epithelial cells. Together with the cytochalasin D treatment, our data revealed that actin polymerization is necessary but not sufficient to polarize centrioles in *Drosophila* wings. Our results suggest that the connection between the actin-based hair and the centriole depends on the Fz-PCP pathway but is independent of known PPEs, so that new downstream players need to be found.

In summary, by using complementary quantitative methods, we found three distinct centriole polarization phenotypes. Under PPE mutant conditions, centriole polarization is delayed, but the final distribution and polarity are completely unaffected (Fig. 4I; Fig. S4K). However, PCP core mutants do not polarize centrioles as they remained mostly centred in the cell (Fig. 4I; Fig. S4K). In contrast, actin polymerization is required both to polarize centrioles and to keep them in a restricted area of the cell (Fig. 4I; Fig. S4K) before and after hair formation. In conclusion, we hypothesize that in *Drosophila* pupal wings there are at least two mechanisms controlling centriole positioning – one a general mechanism governed by actin polymerization and independent of PCP, the main function of which is to maintain centriole positioning, and the other a mechanism controlled by the core PCP pathway in charge of moving the centriole to the proper position. Further experiments will be required to dissect the mechanism behind this off-centred movement downstream of the core PCP pathway.

MATERIALS AND METHODS

Fly strains

Fly lines were cultured and crossed on semi-defined medium and maintained at the indicated temperatures (25°C or 29°C). For RNAi studies, the following lines were used: *Fz* RNAi (VDRC stock 105493/KK), *Vang* RNAi (VDRC stock 7376/GD and 100819/KK), *mwh* (VDRC stock 41514/GD and 45265/GD) *Drok* (VDRC stock 3793/GD and 104675/KK), *fritz* (VDRC stock 103611 and 10088/GD), *ds* (VDRC stock 36219/GD and 4313/GD), *fuzzy* RNAi (VDRC stock 108550/KK), *Cdc42* RNAi (VDRC stock 100794/KK), *Rac1* (VDRC stock 49247/GD), *inturned* (VDRC stock 27252/GD and 103407/KK) and *rho* RNAi (VDRC stock 107502/KK and 51952/GD). For overexpression and RNAi studies, the GAL4/UAS system was used to direct the expression of UAS constructs to distinct wing areas,

Development (2018) 145, dev169326. doi:10.1242/dev.169326

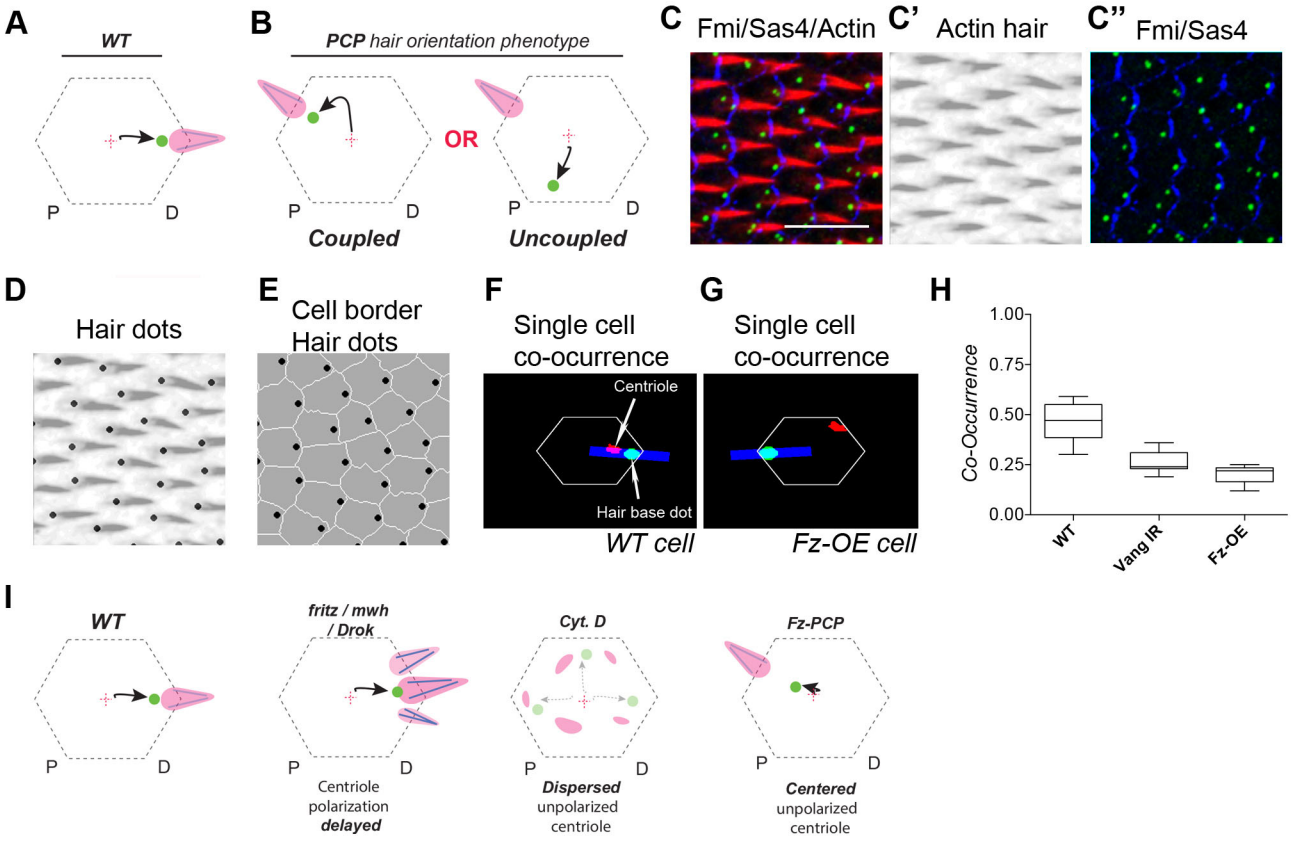

Fig. 4. Centrioles and actin are uncoupled in Fz GOF and Vang LOF conditions. (A,B) Scheme of centriole (green circle) positioning in well-polarized WT cells (A) compared with possible centriole distributions in PCP-induced misorientation conditions, where centrioles can follow (coupled) or not (uncoupled) the base of the actin-hair (pink) (B). (C) Pupal wing expressing Sas4-GFP (green) and labelled with Fmi (blue) and actin (red/grey). (D) Hair dots located at the base of the actin-hair. (E) Hair dots and associated cell borders. (F,G) Snapshot of a single cell co-occurrence analysis in WT (F) and in PCP mutant (G) conditions. (H) In WT cells, centrioles and actin-hairs coincide in the same side of the apical membrane in ~46% of the cells analysed. In contrast, Fz-OE or *vang*-RNAi showed decreased co-occurrence. Box and whiskers represent median and 5-95 percentile. Number of cells>300 (at least 4 wings for each experimental condition). (I) Schematic representation of the phenotypes described in this study, where in WT cells, centrioles (green circles) migrate to base of the actin-hairs (pink region). This centriole migration is delayed but not affected in terms of polarity and distribution in those PPE tested conditions (*fritz*/*mwh*/*Drok*), but it is deeply disturbed by Cyt. D treatment where actin polymerization is affected and under Fz-PCP experimental conditions. D, distal side; P, proximal side. Scale bar: 10 µm.

linked to the localized expression of developmental genes such as *decapentaplegic* (*dpp*), expressed in a central stripe, and *nubbin* (*nub*), expressed in the whole wing. For cytochalasin D experiments, UAS-GFP-CG2919 (Asl) flies were crossed with UAS-dcr^{2}nub-GAL4 to direct the expression of *asterless* coupled to green fluorescent protein (GFP) to the whole wing.

Adult wing analysis

For analysis of wing trichomes, adult wings were removed, incubated in wash buffer [PBS and 0.1% Triton X-100 (PBS-t)] and mounted on a slide in 80% glycerol in PBS. Adult wings were imaged at room temperature using an Olympus BX51 direct microscope. Images were acquired with an Olympus DP72 camera and CellD software (Olympus).

Immunohistochemistry

Pupae were collected from vials at white stage and cultured at 29°C for different time points (25 h or 28.5 h). Pupae were dissected in PBS-t and fixed with 4% paraformaldehyde for 1 h at room temperature. Then, pupae were washed in PBS-t three times for 5 min each wash and blocked in PBS-t with 2% bovine serum albumin (BSA) for 45 min. Samples were incubated with primary antibody overnight at room temperature in PBS-t-BSA. After overnight incubation, samples were washed five times in PBS-t and incubated for 90 min in fluorescent phalloidin to stain F-actin and fluorescent secondary antibodies, both diluted in PBS-t-BSA. To continue the staining, five washes in PBS-t were performed and pupal wings were then detached from the pupal cage. Finally, samples were mounted on slides with medium for fluorescence (Vectashield). To stain the cellular membrane anti-Fmi (also known as Starry night, Stan; from DSHB clone 74, dilution 1:20) was used. Secondary antibody conjugated with the fluorophore Alexa 405 was used at 1:200 (A-31553, Invitrogen) and Alexa 594-phalloidin was used at 1:200 (Invitrogen).

Image acquisition and processing

Pupal wings were oriented with the distal part always pointing to the right side of the image and images were acquired using an Olympus FV 1000 confocal microscope. After acquisition, images were processed using ImageJ (Fiji) to select the wing sections and generate the cell borders mask (Tissue Analyzer plugin), and Adobe Photoshop CC 2015 to create the colour-coded mask based on the number of hairs.

In vitro pupal culture and cytochalasin D treatment

For cytochalasin D treatment, *UAS-GFP-Asl* and *UAS-dcr2;nub-GAL4*, which directs the expression of GFP-*asterless* to the whole wing, were used. White pupae from the crossing were cultured for 25 h at 29°C and removed from the pupal case in aseptic conditions. Dissection was carried in modified M3 medium (MM3) supplemented with 20-hydroxyecdysone at 100 ng/µl (Sigma). Then, each pupa was carried

Development (2018) 145, dev169326. doi:10.1242/dev.169326

separately to 200 µl tubes and cultured at 29°C for 10 h in 100 µl of supplemented MM3 medium. For inhibition of actin polymerization, cytochalasin D was used at 5 ng/µl and treatment was carried out in supplemented MM3 medium in the same conditions. After incubation, pupae were washed in PBS-t for 5 min and the staining was performed as described above.

ABP method

Average basal body position (ABP) for each sample was calculated following the protocol of Hashimoto and colleagues (Hashimoto et al., 2010). Briefly, the score for a specific cell i represents the normalized position of the centriole along the proximo-distal axis (−1.0 being the minimal distal coordinate of the cell, 0 the cell centroid and 1.0 the maximal proximal coordinate of the cell). This score can be quantified as

$$Sc_i = \frac{Cx_i - midx_i}{maxx_i - midx_i},$$

where Cx_i is the x-coordinate of the centriole, $maxx_i$ is the maximum x-coordinate value in the cell i, and $midx_i$ is the x-coordinate centroid value of the cell, following

$$midx_i = \frac{maxx_i + minx_i}{2},$$

where $minx_i$ is the minimum x-coordinate value in the cell i. Finally, the ABP was calculated as the average value of this score across the cells within an image, with higher values indicating polarized centrioles.

Q method

Each centriole was assigned to a specific quartile (Q) depending on their relative position to the anterior-posterior axis of the cell (Taniguchi et al., 2011). Specifically, we drew two virtual lines that crossed the centroid of the cell with a $\pi/4$ and $-\pi/4$ orientation. These lines divided the space of the cell in four different regions. If the centriole position was located between $-\pi/4$ and $\pi/4$, then it was assigned to the Q1 region. If the centriole was located between $\pi/4$ and $3\pi/4$, it was assigned to Q2. In the case of being located between $-\pi/4$ and $-3\pi/4$, then it was assigned to Q3, and, finally, the rest of centrioles were assigned to Q4. A higher proportion of Q1 values represents polarized centrioles.

Imaging pre-processing and generation of single cellular models

Ad hoc MATLAB functions were designed to analyse confocal microscopy images and generate the RPCD model; comparisons between the samples and the co-occurrence analysis can be obtained in our webpage (cellpolaritylab.blogspot.com). Individual cells were identified by the segmentation of the cell membranes that were obtained by CellProfiler. In order to standardize cellular morphologies, each individual cell was modelled as a regular hexagon with a side length l, following the formula

$$l = \sqrt[2]{\frac{2 \times a}{3 \times \sqrt[2]{3}}},$$

where a is the full area in pixels of the individual cell. Then, the intensities of the individual pixels of the cell in each channel were translated to the cellular model by normalizing the original distance of the pixel to the cell centroid to the new radius (l) of the model. Finally, all the individual cell models were resized to a square matrix with sides of 400 pixels and with a regular hexagon (l=100 pixels) located in the centre of the matrix. This method provided us with a collection of RGB matrices that represent individual cells, allowing the comparison or the combination of multiple cells obtained from even different fields or experiments.

Centriole mapping and representative polarized centriole distribution (RPCD)

Using the standard cell models previously described, we found the centrioles by segmentation of the Sas4/Asl signal in the green channel of the cell matrices. This method produces a novel logical matrix C_i for each centriole i, representing the normalized position of the centriole within a cell. A combined view of the position of the centrioles from a set of cells can be obtained by plotting their accumulated density following

$$AD = \sum_{i=1}^{n} \left(\frac{C_i}{tr(E \times C_i)} \right),$$

where i represents the index of the set of n matrices, E is an all-ones matrix with the same dimension of C_i, and tr indicates the trace of the matrix. Note that the divider of this equation represents the total sum of the elements of C_i. This accumulated density represents an intuitive way to visualize centriole position and polarity in a set of cells, as shown in Fig. 3.

In addition to the visualization method, we wanted to design an analytical method to compare centriole location in different conditions. In order to do this, we built a centriole library using the C matrices of a collection of 4526 cells obtained from different fields, wings and experiments of 28.5 APF at 29°C. This library is a good choice to represent the average position of centrioles in a polarized cell, while at the same time it also provides a measure of the technical and biological variability observed in centriole polarization. Thus, we calculated the accumulated density matrix ADL of this library as described in the previous paragraph. We then extracted the areas in which the centrioles are predominantly located by the isolines method. Briefly, isolines (or contour lines) are closed curves in the ADL matrix whose points maintain a constant value k (in our case, k=[6, 7, 8, 9, 10, 11, 12]×10^{-5}). This way, each isoline k delimitates a specific region in ADL in which centrioles are localized at a concrete probability q. This q parameter can be obtained by the intersection of ADL and the IM_k matrix generated from the closed isoline k as follows:

$$q = \frac{\cap(IM_k, ADL)}{n},$$

where n=4526 as it is the number of centrioles included in the library. By using seven different isolines that cover from q=0.4 to q>0.8 in the library of polarized cells, we have established a model for the RPCD in fly wings. For the sake of clarity, in some experiments we have chosen only the isoline 3 (i_3), which determines a 2D region with a percentage of centriole coverage from our library of around 60% (Fig. S5F), although similar results were found using other isolines.

Statistical comparison of a centriole set and the RPCD

The design of this RPCD allowed us to test if an external sample (a Sas4/Asl microscopy image linked with its cell borders) is statistically different to WT polarized conditions. Specifically, we calculated the threshold scores that represent the minimum coverage for a sample with m cells to be present within the IM matrix generated by the isoline k at a specific P-value. To do this, we calculated

$$q_r = \frac{\cap(IM_k, ADr)}{m}$$

for r=[1, 2, 3, …, 1000], where ADr represented the accumulated density matrix obtained using a random selection of m polarized cells. Thus, the 5% percentile of the q_r distribution estimated the minimum threshold q value to reject the null hypothesis (an external sample is less polarized than the WT library) at a P-value=0.05, and we symbolized this parameter as q_{exp05}. Finally, we used as score

$$OER_{05} = \frac{q_{obs}}{q_{exp05}},$$

where q_{obs} represented the q value observed for the external sample at the isoline k. Values of OER_{05} higher or lower than 1 indicated polarized or non-polarized conditions, respectively.

Representative non-polarized centriole distribution (RNCD)

The previous approach was modified to generate a non-polarized centriole library from cells without hair formation. In order to do this, we selected 5129 cells from different fields, wings and experiments from 25 APF wings.

Development (2018) 145, dev169326. doi:10.1242/dev.169326

Then, all the previously described steps were performed (isoline generation and calculation of q_{exp05} for different cell library sizes and isolines) in order to compare centriole samples against a non-polarized model.

Calculation of co-occurrence between actin-rich hairs and centrioles

Using the standard cell models previously described, we estimated the base of the actin hair in a cell by segmentation of an additional, manually curated layer, which assigned a dot to each actin hair. Afterwards, we rotated a fixed-size rectangle (150×20 pixels) around the midpoint of its left side, which was coincident with the centroid of the cell. Thus, we were able to measure the orientation of the rectangle in which we colocalized the base of the actin hair. Then, we simply determined

$$coOc_i \begin{cases} = 1, if\{\cap(C_i, RM_i)\} > 0 \\ = 0, if\{\cap(C_i, RM_i)\} = 0 \end{cases},$$

where RM_i is the matrix determined by a rectangle rotated to localize the base of the actin hair in the cell i. Finally, we calculated the average value of $coOc$ for the n cells in a sample. We also estimated the random level of co-occurrence that can happen in a set of cells, by two different methods. In the first method, we randomly assigned centriole matrices C_i obtained from 25 APF fly wings (not polarized) to rectangle matrices RM from polarized cells, and then we calculated the co-occurrence as before. In the second method, we designated each centriole to a random position within the model cell obtaining random matrices C_{ri}. These were assigned to rectangle matrices RM from polarized cells, as in the first method and co-occurrence was finally calculated.

Statistical analyses

Data were analysed using one-way ANOVA followed by the Bonferroni multiple comparisons post-test (GraphPad Prism) for co-occurrence, Q and ABP methods. In the case of RPCD and RNCD, the data were compared with the model using the OER_{05}, which measures the statistical significance (values below 1 represent a P-value below 0.05) but also using t-test to compare different experimental groups.

Acknowledgements

We are most grateful to Jordan Raff for many reagents and all members of the Carvajal lab for helpful suggestions, comments and discussions during the development and execution of the project. We thank the Bloomington and VDRC Stock Centers for fly strains, and the DSHB for antibodies. Confocal microscopy was performed at the UEX microscopy core facility (Servicio de Técnica Aplicadas a Biociencias, STAB). We thank Dr Francisco Centeno and Dr Sonia Mulero for helpful discussions and comments on the manuscript.

Competing interests

The authors declare no competing or financial interests.

Author contributions

Conceptualization: J.M.C.-G.; Software: A.-C.R.; Formal analysis: A.-C.R.; Investigation: S.G.-J., J.M.C.-G.; Writing - original draft: J.M.C.-G.; Writing - review & editing: S.G.-J., A.-C.R., J.M.C.-G.; Visualization: A.A.-B.; Supervision: J.M.C.-G.; Project administration: J.M.C.-G.; Funding acquisition: J.M.C.-G.

Funding

J. M.C.-G. was a recipient of an 'Atraccion y Retencion de talento' contract from the GOBEX (Extremadura government) and was a recipient of a Ramón y Cajal contract (RYC-2015-17867). This work was supported by grants from the Ministerio de Economía, Industria y Competitividad, Gobierno de España (BFU2014-54699-P, BFU2017-85547-P to J.M.C.-G.) and from Consejería de Economía e Infraestructuras del Gobierno de Extremadura (GR15164). A.-C.R. was a recipient of a Federation of European Biochemical Societies Long-Term Postdoctoral Fellowship. S.G.-J. was a recipient of a Fellowship from the Universidad de Extremadura. All Spanish funding is co-sponsored by the European Regional Development Fund (FEDER) program.

Supplementary information

Supplementary information available online at
http://dev.biologists.org/lookup/doi/10.1242/dev.169326.supplemental

References

Adler, P. N. (2012). The frizzled/stan pathway and planar cell polarity in the Drosophila wing. *Curr. Top. Dev. Biol.* **101**, 1-31.

Adler, P. N. and Wallingford, J. B. (2017). From planar cell polarity to ciliogenesis and back: the curious tale of the PPE and CPLANE proteins. *Trends Cell Biol.* **27**, 379-390.

Almuedo-Castillo, M., Salo, E. and Adell, T. (2011). Dishevelled is essential for neural connectivity and planar cell polarity in planarians. *Proc. Natl. Acad. Sci. USA* **108**, 2813-2818.

Bettencourt-Dias, M., Hildebrandt, F., Pellman, D., Woods, G. and Godinho, S. A. (2011). Centrosomes and cilia in human disease. *Trends Genet.* **27**, 307-315.

Boisvieux-Ulrich, E., Lainé, M.-C. and Sandoz, D. (1990). Cytochalasin D inhibits basal body migration and ciliary elongation in quail oviduct epithelium. *Cell Tissue Res.* **259**, 443-454.

Borovina, A., Superina, S., Voskas, D. and Ciruna, B. (2010). Vangl2 directs the posterior tilting and asymmetric localization of motile primary cilia. *Nat. Cell Biol.* **12**, 407-412.

Brooks, E. R. and Wallingford, J. B. (2014). Multiciliated cells. *Curr. Biol.* **24**, R973-R982.

Carvajal-Gonzalez, J. M. and Mlodzik, M. (2014). Mechanisms of planar cell polarity establishment in Drosophila. *F1000Prime Rep.* **6**, 98.

Carvajal-Gonzalez, J. M., Mulero-Navarro, S. and Mlodzik, M. (2016a). Centriole positioning in epithelial cells and its intimate relationship with planar cell polarity. *BioEssays* **38**, 1234-1245.

Carvajal-Gonzalez, J. M., Roman, A. C. and Mlodzik, M. (2016b). Positioning of centrioles is a conserved readout of Frizzled planar cell polarity signalling. *Nat. Commun.* **7**, 11135.

Collier, S. and Gubb, D. (1997). Drosophila tissue polarity requires the cell-autonomous activity of the fuzzy gene, which encodes a novel transmembrane protein. *Development* **124**, 4029-4037.

Collier, S., Lee, H., Burgess, R. and Adler, P. (2005). The WD40 repeat protein fritz links cytoskeletal planar polarity to frizzled subcellular localization in the Drosophila epidermis. *Genetics* **169**, 2035-2045.

Devenport, D. (2014). The cell biology of planar cell polarity. *J. Cell Biol.* **207**, 171-179.

Eaton, S., Auvinen, P., Luo, L., Jan, Y. N. and Simons, K. (1995). CDC42 and Rac1 control different actin-dependent processes in the Drosophila wing disc epithelium. *J. Cell Biol.* **131**, 151-164.

Eaton, S., Wepf, R. and Simons, K. (1996). Roles for Rac1 and Cdc42 in planar polarization and hair outgrowth in the wing of Drosophila. *J. Cell Biol.* **135**, 1277-1289.

Ezan, J. and Montcouquiol, M. (2013). Revisiting planar cell polarity in the inner ear. *Semin. Cell Dev. Biol.* **24**, 499-506.

Goodrich, L. V. and Strutt, D. (2011). Principles of planar polarity in animal development. *Development* **138**, 1877-1892.

Gray, R. S., Abitua, P. B., Wlodarczyk, B. J., Szabo-Rogers, H. L., Blanchard, O., Lee, I., Weiss, G. S., Liu, K. J., Marcotte, E. M., Wallingford, J. B. et al. (2009). The planar cell polarity effector Fuz is essential for targeted membrane trafficking, ciliogenesis and mouse embryonic development. *Nat. Cell Biol.* **11**, 1225-1232.

Guirao, B., Meunier, A., Mortaud, S., Aguilar, A., Corsi, J.-M., Strehl, L., Hirota, Y., Desoeuvre, A., Boutin, C., Han, Y.-G. et al. (2010). Coupling between hydrodynamic forces and planar cell polarity orients mammalian motile cilia. *Nat. Cell Biol.* **12**, 341-350.

Hashimoto, M., Shinohara, K., Wang, J., Ikeuchi, S., Yoshiba, S., Meno, C., Nonaka, S., Takada, S., Hatta, K., Wynshaw-Boris, A. et al. (2010). Planar polarization of node cells determines the rotational axis of node cilia. *Nat. Cell Biol.* **12**, 170-176.

Jones, C. and Chen, P. (2008). Primary cilia in planar cell polarity regulation of the inner ear. *Curr. Top. Dev. Biol.* **85**, 197-224.

Minegishi, K., Hashimoto, M., Ajima, R., Takaoka, K., Shinohara, K., Ikawa, Y., Nishimura, H., McMahon, A. P., Willert, K., Okada, Y. et al. (2017). A Wnt5 activity asymmetry and intercellular signaling via PCP proteins polarize node cells for left-right symmetry breaking. *Dev. Cell* **40**, 439-452.e434.

Mitchell, B., Stubbs, J. L., Huisman, F., Taborek, P., Yu, C. and Kintner, C. (2009). The PCP pathway instructs the planar orientation of ciliated cells in the Xenopus larval skin. *Curr. Biol.* **19**, 924-929.

Ohata, S. and Alvarez-Buylla, A. (2016). Planar organization of multiciliated Ependymal (E1) cells in the brain ventricular epithelium. *Trends Neurosci.* **39**, 543-551.

Park, W. J., Liu, J., Sharp, E. J. and Adler, P. N. (1996). The Drosophila tissue polarity gene inturned acts cell autonomously and encodes a novel protein. *Development* **122**, 961-969.

Park, T. J., Haigo, S. L. and Wallingford, J. B. (2006). Ciliogenesis defects in embryos lacking inturned or fuzzy function are associated with failure of planar cell polarity and Hedgehog signaling. *Nat. Genet.* **38**, 303-311.

Park, T. J., Mitchell, B. J., Abitua, P. B., Kintner, C. and Wallingford, J. B. (2008). Dishevelled controls apical docking and planar polarization of basal bodies in ciliated epithelial cells. *Nat. Genet.* **40**, 871-879.

Development (2018) 145, dev169326. doi:10.1242/dev.169326

Peng, Y. and Axelrod, J. D. (2012). Asymmetric protein localization in planar cell polarity: mechanisms, puzzles, and challenges. *Curr. Top. Dev. Biol.* **101**, 33-53.

Reiter, J. F. and Leroux, M. R. (2017). Genes and molecular pathways underpinning ciliopathies. *Nat. Rev. Mol. Cell Biol.* **18**, 533-547.

Shi, D., Komatsu, K., Hirao, M., Toyooka, Y., Koyama, H., Tissir, F., Goffinet, A. M., Uemura, T. and Fujimori, T. (2014). Celsr1 is required for the generation of polarity at multiple levels of the mouse oviduct. *Development* **141**, 4558-4568.

Shi, D., Usami, F., Komatsu, K., Oka, S., Abe, T., Uemura, T. and Fujimori, T. (2016). Dynamics of planar cell polarity protein Vangl2 in the mouse oviduct epithelium. *Mech. Dev.* **141**, 78-89.

Singh, J. and Mlodzik, M. (2012). Planar cell polarity signaling: coordination of cellular orientation across tissues. *Wiley Interdiscip. Rev. Dev. Biol.* **1**, 479-499.

Song, H., Hu, J., Chen, W., Elliott, G., Andre, P., Gao, B. and Yang, Y. (2010). Planar cell polarity breaks bilateral symmetry by controlling ciliary positioning. *Nature* **466**, 378-382.

Spassky, N. and Meunier, A. (2017). The development and functions of multiciliated epithelia. *Nat. Rev. Mol. Cell Biol.* **18**, 423-436.

Taniguchi, K., Maeda, R., Ando, T., Okumura, T., Nakazawa, N., Hatori, R., Nakamura, M., Hozumi, S., Fujiwara, H. and Matsuno, K. (2011). Chirality in planar cell shape contributes to left-right asymmetric epithelial morphogenesis. *Science* **333**, 339-341.

Wong, L. L. and Adler, P. N. (1993). Tissue polarity genes of Drosophila regulate the subcellular location for prehair initiation in pupal wing cells. *J. Cell Biol.* **123**, 209-221.